A comparison of stellar atmospheric parameters from the LAMOST and APOGEE datasets

Yu-Qin Chen[1], Gang Zhao[1], Chao Liu[1], Jing Ren[1], Yun-Peng Jia[1], Jing-Kun Zhao[1], A-Li Luo[1], Yue Wu[1], Yong Zhang[2], Yong-Hui Hou[2], Yue-Fei Wang[2] and Ming Yang[1]

[1] Key Laboratory of Optical Astronomy, National Astronomical Observatories, Chinese Academy of Sciences, Beijing 100012, China; *cyq@bao.ac.cn*
[2] Nanjing Institute of Astronomical Optics & Technology, National Astronomical Observatories, Chinese Academy of Sciences, Nanjing 210042, China

Abstract We have compared stellar parameters, including temperature, gravity and metallicity, for common stars in the LAMOST DR2 and SDSS DR12/APOGEE datasets. It is found that the LAMOST dataset provides a more well-defined red clump feature than the APOGEE dataset in the $T_{\rm eff}$ versus $\log g$ diagram. With this advantage, we have separated red clump stars from red giant stars, and attempt to establish calibrations between the two datasets for the two groups of stars. The results show that there is a good consistency in temperature with a calibration close to the one-to-one line, and we can establish a satisfactory metallicity calibration of $[{\rm Fe/H}]_{\rm APOGEE} = 1.18[{\rm Fe/H}]_{\rm LAMOST} + 0.11$ with a scatter of ~ 0.08 dex for both the red clump and red giant branch samples. For gravity, there is no correlation for red clump stars between the two datasets, and scatters around the calibrations of red giant stars are substantial. We found two main sources of scatter in $\log g$ for red giant stars. One is a group of stars with $0.00253 \times T_{\rm eff} - 8.67 < \log g < 2.6$ located in the forbidden region, and the other is the contaminated red clump stars, which could be picked out from the unmatched region where stellar metallicity is not consistent with position in the $T_{\rm eff}$ versus $\log g$ diagram. After excluding stars in these two regions, we have established two calibrations for red giant stars, $\log g_{\rm APOGEE} = 0.000615 \times T_{\rm eff, LAMOST} + 0.697 \times \log g_{\rm LAMOST} - 2.208$ ($\sigma = 0.150$) for $[{\rm Fe/H}] > -1$ and $\log g_{\rm APOGEE} = 0.000874 \times T_{\rm eff, LAMOST} + 0.588 \times \log g_{\rm LAMOST} - 3.117$ ($\sigma = 0.167$) for $[{\rm Fe/H}] < -1$. The calibrations are valid for stars with $T_{\rm eff} = 3800 - 5400$ K and $\log g = 0 - 3.8$ dex, and are useful in work aiming to combine the LAMOST and APOGEE datasets in a future study. In addition, we find that an SVM method based on asteroseismic $\log g$ is a good way to greatly improve the accuracy of gravity for these two regions, at least in the LAMOST dataset.

Key words: stars: late type — stars: fundamental parameters — stars: atmospheres — stars: abundances

1 INTRODUCTION

A stellar spectroscopic survey provides an important source of knowledge in astrophysics. The information available from spectroscopy includes physical parameters of stars (temperatures, gravities and detailed chemical composition) and their kinematics (radial velocities), which are crucial for our understanding of stars and stellar populations in the Milky Way and other galaxies. The advent of large stellar spectroscopic surveys like SEGUE/SDSS (Yanny et al. 2009), RAVE (Kordopatis et al. 2013), APOGEE (Majewski et al. 2015, in preparation), and LAMOST (Zhao et al. 2012) is leading Galactic astronomy to become a precision science, where we can identify different sub-populations by combining the chemical composition with kinematics and trace Galactic evolution and stellar structure at various Galactic locations in detail.

Recently, the LAMOST telescope, a Wang-Su Reflecting Schmidt Telescope also known as the Guo Shou Jing Telescope (Cui et al. 2012; Liu et al. 2015), has finished a two year regular survey after a one year pilot survey in 2011. The combination of a large aperture (4 m) and high multiplexing ability (4000 fibers) with a 5 degree field of view makes it a unique facility. With low resolution ($R = 1800$), the LAMOST project (Liu et al. 2015) currently provides spectra of $\sim 4\,136\,000$ objects and stellar parameters for $\sim 2\,200\,000$ stars in its second data release (DR2) (Luo et al. 2015, in preparation). This dataset includes many previously observed *Kepler* targets provided by the LAMOST-*Kepler* project (De Cat et al. 2014). More detailed information on the data release can be found in the website (*http://www.lamost.org/public/*). Stellar parameters in the LAMOST DR2 dataset are derived by the package $ULySS$ (Wu et al. 2014; Luo et al. 2015, in preparation), where an observed spectrum is fitted against a model expressed as a linear combination of nonlinear components, optionally convolved with a line-of-sight velocity distribution and multiplied by a polynomial function.

Coincidentally, APOGEE (Majewski et al. 2015, in preparation) has released its three-year, near-infrared survey of 100 000 red giant stars included as part of SDSS-III (Eisenstein et al. 2011; Ahn et al. 2012). With a resolving power of 22 500, APOGEE is able to derive detailed abundances for 15 elements as well as the three basic stellar parameters, temperature, gravity and metallicity. Based on a synthetic grid of Kurucz models and an efficient search method, a best match within the synthetic grid is found for each APOGEE spectrum to provide the initial set of parameters: $T_{\rm eff}$, $\log g$, [M/H], [C/M], [N/M] and [α/M]. Then the stellar parameters are calibrated by giants in the *Kepler* field and stars in clusters.

The main population of observed targets in both the LAMOST and APOGEE surveys is the Galactic disk. In principle, these two surveys can be merged together to probe properties of the Galactic disk, and the results obtained from either one can be checked in an independent way. However, the two surveys are quite different in many ways. They have different observed bands and resolving powers of spectra, and thus they can provide abundances for different elements and kinematics with different precisions. The two surveys have their own advantages in terms of sky coverage, selection function and stellar spectral type. Thus, it is important to combine these different types of information together in order to understand the history of the Galactic disk from different perspectives as well as check if the results from either survey are reliable or not. In view of this, we aim to do a systematic study on the chemical and kinematic properties of the Galactic disk by combining data from the two surveys in the near future. This combination is particularly important for the study of the local effect of chemical evolution, stellar migration in the Galactic disk and the origins of many kinematical structures in the Galactic disk.

It is interesting to know how consistent stellar parameters are from the LAMOST and APOGEE datasets, and if it is possible to establish some kind of transformation relations for stellar parameters between the two datasets so that they can be combined in a future study on the Galaxy. Since the APOGEE dataset is based on high resolution spectra with high signal-to-noise ratios, it may provide better parameters, at least for stellar metallicity, than the LAMOST dataset, which is estimated from

low resolution and low signal-to-noise spectra. Moreover, we hope to check the stellar parameters provided by the LAMOST DR2 dataset before they can be effectively used to probe the evolution of the Galaxy. Specifically, we want to know what kinds of stars in the LAMOST DR2 dataset have reliable parameters, and what kinds of stars show unreasonable values which should be excluded in a future study of the Galaxy. Finally, this check and comparison might reveal some clues to improve the stellar parameters provided by both the LAMOST DR2 and APOGEE datasets. In this work, we aim to select a sample of common stars with high quality spectra in both datasets, compare stellar parameters and establish calibrations for individual stellar parameters if possible.

Section 2 provides the star sample and its division into two subsamples, and Section 3 gives a comparison of stellar parameters and the calibrations between the LAMOST DR2 and SDSS DR12/APOGEE datasets. The summary of this comparison is given in Section 4.

2 STAR SAMPLE AND ITS DIVISION INTO RC AND RGB SUBSAMPLES

The selection procedure of the sample stars is applied as follows. First, we select common stars with the same coordinates, such that their (RA, DEC) should be within 3 arcsecs, in the LAMOST DR2 and SDSS DR12/APOGEE datasets. Then we apply the restriction of stars having stellar parameters in reasonable regions of $3000 < T_{\rm eff} < 9000\,{\rm K}$, $-1.0 < \log g < 6.0$ and $-5.0 < [{\rm Fe/H}] < 1.0$. Third, we select stars with high signal-to-noise ratio (SNR) spectra in both surveys; the SNR in g band of LAMOST spectra should be > 30 and the SNR of APOGEE spectra should be > 100. With these criteria, we have 5626 stars in common, for which the $T_{\rm eff}$ versus $\log g$ diagrams are shown in Figure 1. We notice that there are some turn-off and subgiant stars. Since the APOGEE dataset only provides stellar parameters for giants, we thus limit our sample to stars with $\log g < 3.8$ in both datasets. In total, we have 5352 stars for comparison.
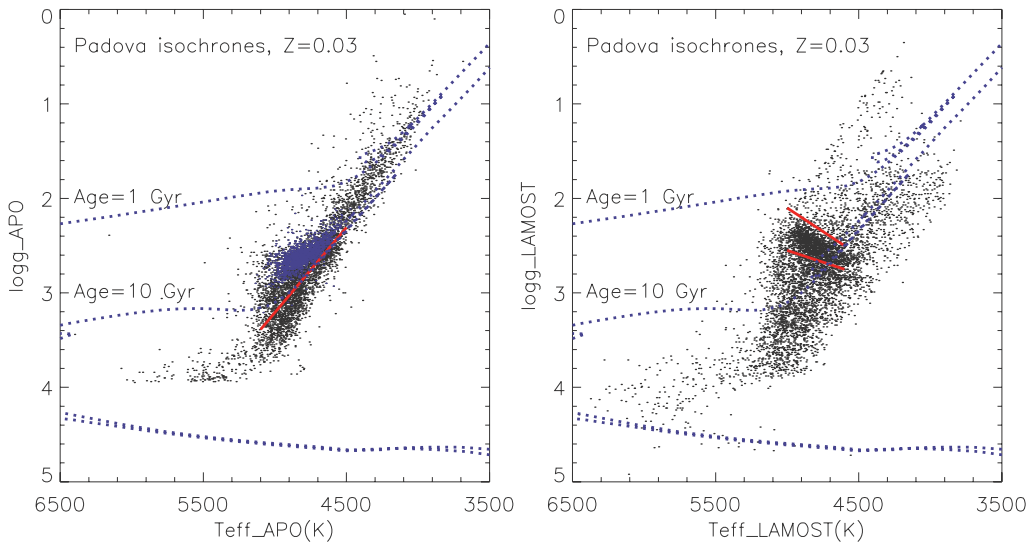
Fig. 1 The $T_{\rm eff}$ versus $\log g$ diagrams for the LAMOST (*right panel*) and APOGEE (*left panel*) datasets based on 5626 common stars with high quality spectra (LAMOST: SNR> 30, APOGEE: SNR> 100). Dashed lines show theoretical isochrones representing 1 and 10 Gyr at $Z = 0.030$ from the Padova website (Bressan et al. 2012). The selection criteria for RC stars are marked in red lines, and blue dots in the left panel are our sample of RC stars selected from the LAMOST dataset.

There are some differences in the $T_{\rm eff}$ versus $\log g$ diagrams between the two datasets. The most prominent difference is that the LAMOST dataset shows a strong clump feature in this diagram which corresponds to the well-known red clump (RC) population, which is not easily seen by eye in data from the APOGEE dataset. The appearance of this feature demonstrates that stellar parameters calculated from the LAMOST dataset are generally reasonable, at least for stars at this region. With this advantage, we select a sample of RC stars from the LAMOST dataset which is limited to stars within the two red lines, where stars follow the relation $-0.0010 \times T_{\rm eff,LAMOST} + 7.10 < \log g_{\rm LAMOST} < -0.0005 \times T_{\rm eff,LAMOST} + 5.05$ and are in the temperature range $4600 < T_{\rm eff,LAMOST} < 5000\,{\rm K}$. The right temperature limit of $T_{\rm eff,LAMOST} < 5000\,{\rm K}$ is applied since the number of stars significantly decreases in the right panel of Figure 1, and this criterion may exclude the secondary RC sequence, which is predicted to be located on the blue and faint-magnitude side of the main RC sequence in the color magnitude diagram (CMD) (Girardi 1999). The left temperature limit of $T_{\rm eff,LAMOST} > 4600\,{\rm K}$ is chosen in order to avoid contamination from the possible bump in the RGB at the red side of the RC that has solar metallicity. For comparison, two theoretical isochrones representing 1 Gyr and 10 Gyr with $Z = 0.030$ from the Padova website (*http://stev.oapd.inaf.it/cgi-bin/cmd*, Bressan et al. 2012) are overplotted in Figure 1.

The selection procedure for the RC sample is mainly based on a check by eye of the $T_{\rm eff}$ versus $\log g$ diagram of the LAMOST dataset. According to Bovy et al. (2014), RC stars in the APOGEE dataset can be selected by their position in color-metallicity-gravity-temperature space using a new method calibrated using stellar evolution models and high-quality asteroseismology data. In their figure 1, a linear line of $\log g_{\rm APOGEE} = 0.0018 \times (T_{\rm eff,APOGEE} - 4607) + 2.5$ at solar metallicity clearly separates RC stars from RGB stars, which is shown as the red line in the left panel of Figure 1. When we overplot our selected RC sample of stars with blue dots in the $T_{\rm eff}$ versus $\log g$ diagram of the APOGEE dataset, they are located exactly on the left edge of the red line. Thus, our RC sample generally follows the selection criteria of Bovy et al. (2014). Note that our RC sample stars do not take into account stars on the secondary RC sequence for two reasons. First, they can be identified by asteroseismic analysis (Stello et al. 2013) but it is difficult to pick them out from the $T_{\rm eff}$ versus $\log g$ diagram. Secondly, they might have different properties as compared with stars on the main RC sequence; they are massive, young and have different dependences of $\log g$ with $T_{\rm eff}$. Thus, this work mainly involves the main sequence RC stars. Finally, we divide our selected sample of 5352 stars into two samples, the RC sample with 1544 stars and the RGB sample from the remaining 3808 stars. In the following sections, the two samples will be investigated separately due to their different properties.

3 A COMPARISON OF STELLAR PARAMETERS FROM THE LAMOST AND APOGEE DATASETS

3.1 The $T_{\rm eff}$, $\log g$ and [Fe/H] Distributions

In order to investigate if there is any systematic shift in stellar parameters between the LAMOST and APOGEE datasets, we show the distributions of $T_{\rm eff}$, $\log g$ and [Fe/H] in Figure 2 for both samples. They demonstrate that there are systematic shifts in the $\log g$ and [Fe/H] distributions but there is not a clear difference in the $T_{\rm eff}$ distribution between the two datasets. For gravity, the LAMOST dataset shows one peak at $\log g \sim 2.3-2.4$, while the APOGEE dataset has a main peak at $\log g \sim 2.5-2.6$ and a possible second peak at $\log g \sim 2.85$, which may correspond to the secondary RC sequence according to Bovy et al. (2014). For metallicity, there is a prominent shift in the metallicity peak from [Fe/H] ~ -0.1 in the APOGEE dataset to [Fe/H] ~ -0.3 in the LAMOST dataset as well as a shift in the whole distribution toward the metal rich side. In addition, most stars have metallicity in the range $-1.0 < $ [Fe/H] < 0.5 indicating they are the dominate population of the Galactic disk in our sample. Note that the adopted $\log g$ and [Fe/H] values in the APOGEE dataset have been
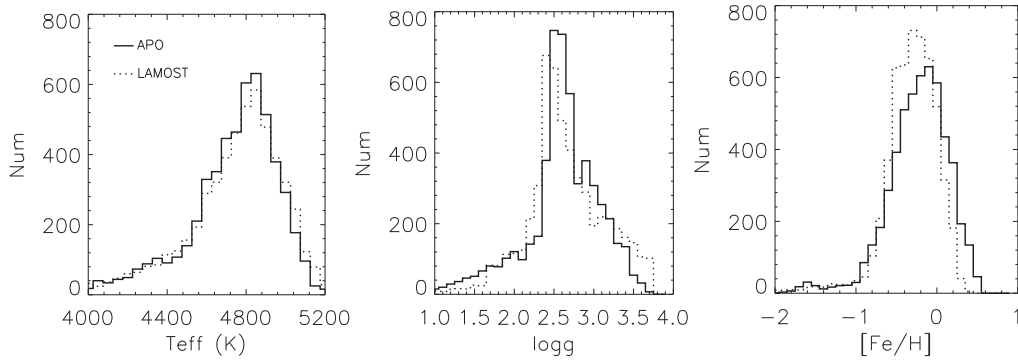
Fig. 2 The distributions of T_{eff}, $\log g$ and [Fe/H] for the whole sample based on the LAMOST (*dashed lines*) and APOGEE (*solid lines*) datasets.
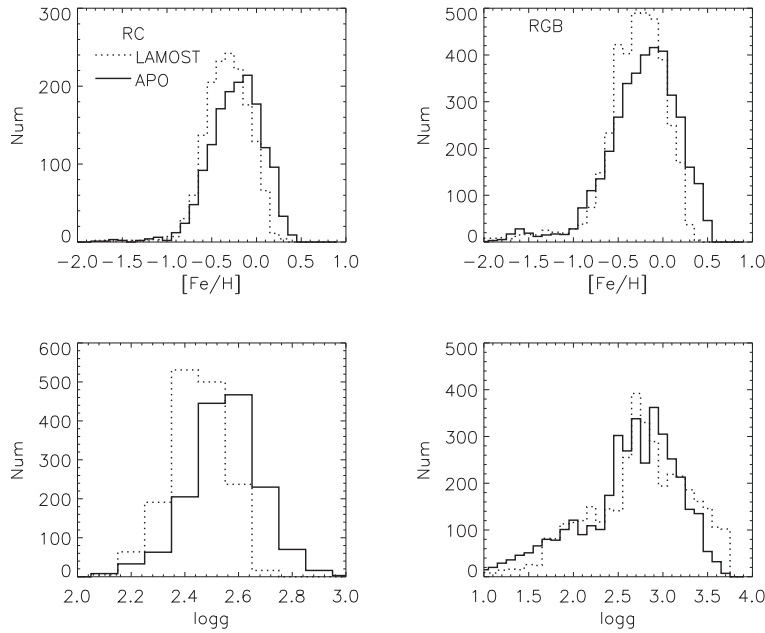
Fig. 3 The distributions of $\log g$ and [Fe/H] for RC (*left*) and RGB (*right*) stars based on the LAMOST (*dashed lines*) and APOGEE (*solid lines*) datasets.

corrected by equations (3) and (6) in Holtzman et al. (2015), without which the differences between the two datasets would be even larger.

Figure 3 shows the [Fe/H] and $\log g$ distributions for both the RC and RGB samples. Clearly, the shift in metallicity is systematic, and the RC and RGB samples behave in a similar way. The systematic shift of gravity in Figure 2 mainly comes from the RC sample, but it is not so prominent in the RGB sample. Instead, the APOGEE dataset shows a slightly broader $\log g$ distribution than the LAMOST dataset. Moreover, as shown in Figure 1, the dependence of $\log g$ with T_{eff} in the RC sample shows opposite trends in the LAMOST and APOGEE datasets. In view of these different

properties for RC and RGB samples, it is reasonable to establish calibrations for RC and RGB stars separately.

3.2 The Comparison and Calibrations of Stellar Parameters

If possible, we aim to establish the calibrations of stellar parameters from the LAMOST and APOGEE datasets in order to combine these two surveys in a future study. For this purpose, the one-to-one comparisons between the LAMOST and APOGEE datasets of $T_{\rm eff}$, $\log g$ and [Fe/H] for the RC (left panels) and RGB (right panels) samples are shown in Figure 4. Stars with [Fe/H] < -1 are marked by red crosses since they only contribute small amounts to our main population from the Galactic disk with [Fe/H] > -1 (see Fig. 2).

Note that most stars in our RC sample have [Fe/H] > -0.8 which is consistent with the metallicity distribution of local RC stars as shown in Puzeras et al. (2010). However, 22 stars in our RC sample have [Fe/H] < -1, which is outside the metallicity range of the local RC sample of
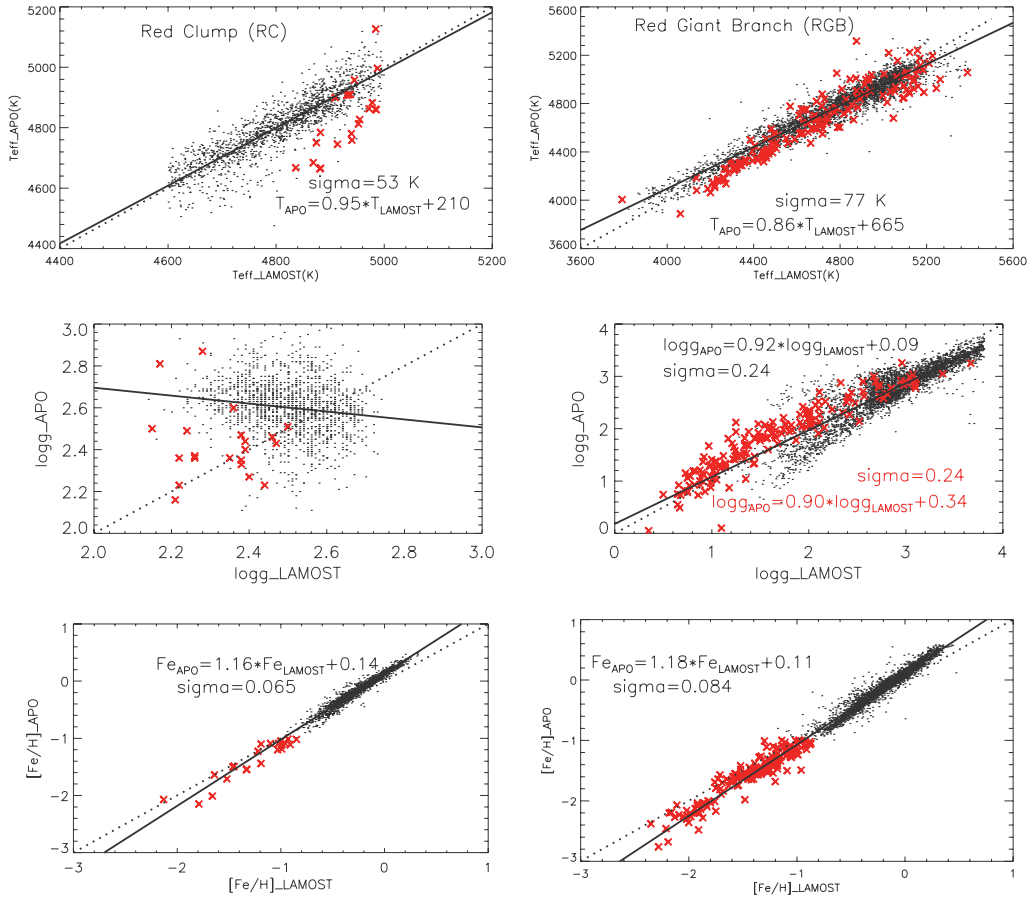
Fig. 4 The comparisons and calibrations of $T_{\rm eff}$, $\log g$ and [Fe/H] between the LAMOST and APOGEE datasets for the RC (*left panels*) and RGB (*right panels*) samples. Dashed lines are the one-to-one relations while solid lines are the calibrations. Stars with [Fe/H] < -1 are indicated by red crosses.

$-0.8 <$ [Fe/H] < 0.3 (their fig. 5). We marked these RC stars with [Fe/H] < -1 by red crosses in the left panels of Figure 4. We find that they do not follow the general trends of most RC stars in both the $T_{\rm eff}$ and $\log g$ panels of Figure 4. Thus, they might not be real RC stars. Instead, they could be red horizontal branch or metal poor red giant stars, but it is difficult for us to distinguish them. Thus, these stars are excluded in the following analyses. For RC stars, the agreement in $T_{\rm eff}$ between the LAMOST and APOGEE datasets is good with a scatter of 53 K around the calibration of $T_{\rm eff,APOGEE} = 0.95 \times T_{\rm eff,LAMOST} + 210$. Note that significant deviations in the temperature comparison from the one-to-one line at both ends mainly come from the selection criterion of $4600 < T_{\rm eff,LAMOST} < 5000$ K for RC stars. However, there is neither any correlation nor any kind of anticorrelation in the $\log g$ comparison, and the scatters are too large to obtain reliable calibrations. For metallicity, a good calibration of $[{\rm Fe/H}]_{\rm APOGEE} = 1.16 \times [{\rm Fe/H}]_{\rm LAMOST} + 0.14$ with a scatter of 0.065 dex can be established for RC stars with [Fe/H] > -1.

For RGB stars, a metallicity calibration of $[{\rm Fe/H}]_{\rm APOGEE} = 1.18 \times [{\rm Fe/H}]_{\rm LAMOST} + 0.11$ ($\sigma = 0.08$) that is similar to the RC sample is found, and we may establish a $T_{\rm eff}$ calibration of $T_{\rm eff,APOGEE} = 0.86 \times T_{\rm eff,LAMOST} + 665$ with a scatter of 77 K. For gravity, the general trend in the comparison follows the one-to-one line, but there are very large scatters in the range $1.5 < \log g_{\rm LAMOST} < 2.6$. Moreover, stars with [Fe/H] < -1, again marked by red crosses, have a systematically higher value by ~ 0.2 dex for stars with $\log g_{\rm LAMOST} > 1.0$. In view of this difference, we establish two gravity calibrations for RGB stars with a metallicity division at [Fe/H] $= -1$, $\log g_{\rm APOGEE} = 0.92 \times \log g_{\rm LAMOST} + 0.09$ for [Fe/H] > -1 and $\log g_{\rm APOGEE} = 0.90 \times \log g_{\rm LAMOST} + 0.34$ for [Fe/H] < -1, with a scatter of 0.24 in both calibrations. When the temperature term is included, the scatters are slightly reduced with calibrations of $\log g_{\rm APOGEE} = 0.00105 \times T_{\rm eff,LAMOST} + 0.46 \times \log g_{\rm LAMOST} - 3.85$ ($\sigma = 0.20$) for [Fe/H] < -1 and of $\log g_{\rm APOGEE} = 0.00087 \times T_{\rm eff,LAMOST} + 0.59 \times \log g_{\rm LAMOST} - 3.11$ ($\sigma = 0.17$) for [Fe/H] > -1. When we further include the metallicity term, the calibrations are $\log g_{\rm APOGEE} = 0.00140 \times T_{\rm eff,LAMOST} + 0.28 \times \log g_{\rm LAMOST} + 0.20 \times [{\rm Fe/H}]_{\rm LAMOST} - 4.89$ ($\sigma = 0.20$) for [Fe/H] < -1 and $\log g_{\rm APOGEE} = 0.00107 \times T_{\rm eff,LAMOST} + 0.46 \times \log g_{\rm LAMOST} + 0.34 \times [{\rm Fe/H}]_{\rm LAMOST} - 3.64$ ($\sigma = 0.15$) for [Fe/H] > -1.

3.3 Refining the $\log g$ Calibrations for RGB Stars with [Fe/H] > -1

In order to probe the large scatter in the $\log g$ calibration between the APOGEE and the LAMOST datasets for RGB stars, we carefully inspect their differences in the $T_{\rm eff}$ versus $\log g$ diagrams in the top panels of Figure 5. These show that the main discrepancy comes from the lack of stars on the right side of the blue dashed line, which can be expressed by the relation $\log g = 0.00253 \times T_{\rm eff} - 8.67$ which intersects the two points (3500,0.2) and (5000,4.0) in the plot of ($T_{\rm eff}$,$\log g$). The solid line in the upper-left panel of Figure 5 shows an extreme case with an isochrone representing 16 Gyr at the metallicity of $Z = 0.030$ from the Padova group (Bressan et al. 2012), and we find a substantial number of stars in the LAMOST dataset are located on the right side of this extreme case. We thus define a forbidden region where no theoretical model can predict that these stellar parameters exist. Taking temperature and gravity uncertainties into account as well as the theoretical isochrone representing 16 Gyr at $Z = 0.030$, we may assign stars with $\log g_{\rm LAMOST} < 2.6$ from the LAMOST dataset that are located on the right side of the blue line as belonging to a forbidden region; they are marked by blue dots in all panels of Figure 5. Obviously, these blue dots are located below the one-to-one line in the comparison of $\log g$ in the lower left panel of Figure 5, indicating the LAMOST values are very high compared to the APOGEE values. These stars become one of the main sources of scatter shown by $\log g$ in the comparison, and thus they should be excluded from the calibrations.

Meanwhile, recall that our selection criteria of RC stars are quite strict in order to obtain a clear sample, and thus our RGB sample from the remaining stars is somewhat contaminated by some RC stars. In particular, the secondary RC stars, if they exist, are located on the blue side of the main
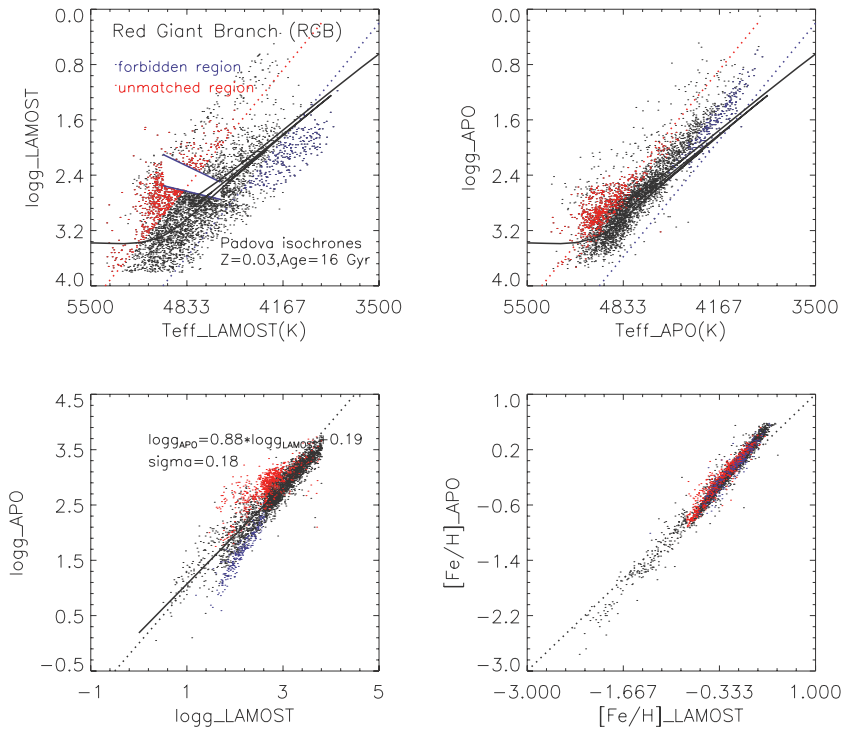
Fig. 5 *Upper*: The T_{eff} versus $\log g$ diagrams for RGB stars in the LAMOST and APOGEE datasets. The blue dashed line which intersects two points at $(T_{\mathrm{eff}}, \log g)$ values of $(3500,0.2)$ and $(5000,4.0)$ and the black solid line is the isochrone of 16 Gyr at $Z = 0.030$ from the Padova group (Bressan et al. 2012). *Lower*: The comparison of gravity and metallicity for different groups of RGB stars. Stars with $2.6 > \log g > 0.00253 \times T_{\mathrm{eff}} - 8.67$ in the forbidden region are marked by blue dots and stars in the unmatched region are marked by red dots.

RC sequence and are included in our RGB sample. We notice that these stars can be distinguished by matching their locations in the T_{eff} versus $\log g$ diagram with their metallicities in the sense that metal poor RGB stars with [Fe/H] < -1 will be located on the blue side of the red dashed line, which arbitrarily shifts the blue line by 400 K in temperature. We do not adopt the theoretical isochrone representing 16 Gyr at the metallicity of $Z = 0.030$ from the Padova group (Bressan et al. 2012) because they do not statistically fit the LAMOST dataset. However, we have checked that the shift of 400 K in temperature corresponds to a change in RGB ridge lines from solar metallicity to [Fe/H] $= -1$. Specifically, stars with [Fe/H] > -1 but which are located on the blue side of the red dashed line could be RC stars instead of RGB stars or RGB stars with the wrong stellar parameters. These stars are marked by red dots in Figure 5, and they constitute the second main source of scatter in the $\log g$ comparison. Generally, they have higher $\log g$ values in the APOGEE dataset than those of the LAMOST datasets. These stars are further excluded from the calibration.

After excluding stars from the above two regions, we repeat the procedures and obtain the calibration of $\log g_{\mathrm{APOGEE}} = 0.000615 \times T_{\mathrm{eff,LAMOST}} + 0.697 \times \log g_{\mathrm{LAMOST}} - 2.208 (\sigma = 0.150)$ for RGB stars with [Fe/H] > -1. The same procedures that are performed for the APOGEE dataset are also applied to the LAMOST dataset, and we obtain the calibration of $\log g_{\mathrm{LAMOST}} = -0.000941 \times T_{\mathrm{eff,APOGEE}} + 1.344 \times \log g_{\mathrm{APOGEE}} + 3.674 (\sigma = 0.167)$ for [Fe/H] > -1.

3.4 On the Gravity Discrepancy of RC Stars

As described in Holtzman et al. (2015), RC stars in the APOGEE dataset are calibrated with the same equation (eq. (3) in that article) as RGB stars. This is not the best solution for RC stars. Instead, a comparison of $\log g$ between the raw ASPCAP values (García et al. 2015, in preparation) and the asteroseismic ones from the APOKASC catalog (Pinsonneault et al. 2014) for targets in the *Kepler* field indicates a difference of 0.15 dex between RC and RGB stars (Holtzman et al. 2015). That means we need to reduce $\log g$ in the APOGEE dataset by a further 0.15 dex for RC stars. If this difference is applied, the $\log g$ distributions between the LAMOST and APOGEE datasets in the lower left panel of Figure 3 are consistent. This consistency shows that the LAMOST $\log g$ for RC stars is on the same scale as that of the asteroseismic values from the *Kepler* survey.

The second discrepancy between the LAMOST and the APOGEE datasets shown by RC stars (see Fig. 1) is the opposite dependence of $\log g$ on $T_{\rm eff}$. In the LAMOST dataset, $\log g$ increases with decreasing $T_{\rm eff}$ with a slope of -0.68 dex per 1000 K, while the slope is 0.89 dex per 1000 K in the APOGEE dataset. This discrepancy is the same if we limit stars to have [Fe/H] > -0.5 in both samples. Since the selection of RC stars is carried out on the LAMOST dataset and we limit stars in the LAMOST temperature range to be $4600 < T_{\rm eff} < 5000$ K, the slope of -0.68 dex per 1000 K just reflects our selection criterion of $-0.0010 \times T_{\rm eff,LAMOST} + 7.10 < \log g_{\rm LAMOST} < -0.0005 \times T_{\rm eff,LAMOST} + 5.05$. Moreover, the slope will be reduced after excluding a few stars at $T_{\rm eff} \sim 4980$ K and $\log g \sim 2.1$, and the scatter of 0.10 dex in $\log g$ at a given $T_{\rm eff}$ will significantly affect this slope. However, there is a strong dependence of $\log g$ on $T_{\rm eff}$ in the APOGEE dataset, which cannot be explained by its scatter. The strong dependence of $\log g$ on $T_{\rm eff}$ persists even though the systematic shift of 0.15 dex is applied to RC stars in the APOGEE dataset.

Since our sample of RC stars fits the selection criteria of Bovy et al. (2014) well, we can expect that they are real RC stars in both datasets. With this understanding, we plot an independent sample of RC stars from Casagrande et al. (2014) by red open circles in Figure 6 and compare the dependence trends of $\log g$ on $T_{\rm eff}$ among the three datasets. Note that the RC sample in Casagrande et al. (2014) has several advantages. (i) RC stars are identified by asteroseismic data with period spacing from Stello et al. (2013) and they have accurate asteroseismic $\log g$. (ii) They have Strömgren $(b-y)_0$ colors, which are very sensitive to temperature. (iii) Casagrande et al. (2014) provide mass and age for RC stars, which allow us to limit stars to have $mass < 1.8 M_\odot$ and $age > 2$ Gyr in order to exclude the RC stars on the secondary sequence. Clearly, there is no slope in the $T_{\rm eff}$ versus $\log g$ diagram, and most stars have $\log g = 2.4 - 2.6$. The LAMOST data show a better agreement with Casagrande et al. (2014) for RC stars than the APOGEE dataset. From a careful inspection of figure 4 in Holtzman et al. (2015), there is a hint of an increasing trend of $\Delta \log g ({\rm ASPCAP} - Kelper)$ with increasing $\log g_{\rm ASPCAP}$ for RC stars (blue squares). If this trend is applied to the APOGEE dataset, the slope in the $T_{\rm eff}$ versus $\log g$ diagram for RC stars in the APOGEE datasets will be slightly reduced. However, further work on this correction should be done in the future.

3.5 New LAMOST Gravities from SVM with Asteroseismic Data

As described above, the LAMOST dataset does not provide the best gravities for giant stars in the forbidden region and the slope in the $T_{\rm eff}$ versus $\log g$ diagram for RC stars is not consistent with that from the SAGA survey by Casagrande et al. (2014). Is there some way to improve these gravities? Recently, Liu et al. (2015, submitted to ApJ) presented a support vector machine (hereafter SVM) method to derive gravities for LAMOST giants based on a sample of stars with asteroseismic $\log g$ in Huber et al. (2014) as a training dataset. In this training dataset, $\log g$ values in Huber et al. (2014) have been re-calculated with the LAMOST $T_{\rm eff}$, and thus these new gravities in Liu et al. (2015, submitted to ApJ) match $T_{\rm eff}$ values in the LAMOST dataset used in the present work.
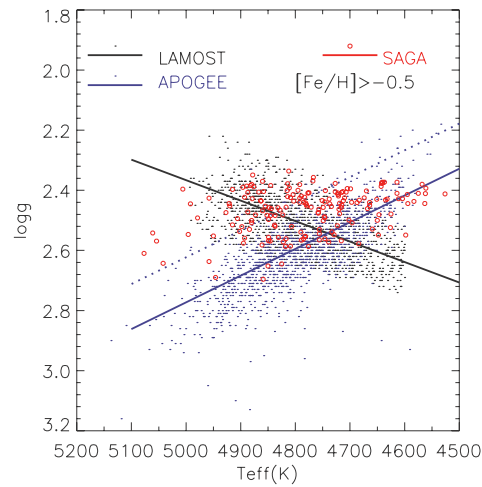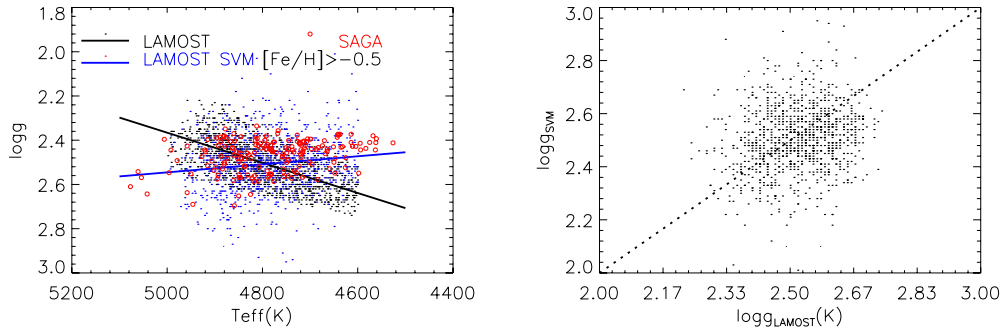
Fig. 6 A comparison of the T_{eff} versus $\log g$ diagram for RC stars in the LAMOST and APOGEE datasets with that from the SAGA survey by Casagrande et al. (2014).
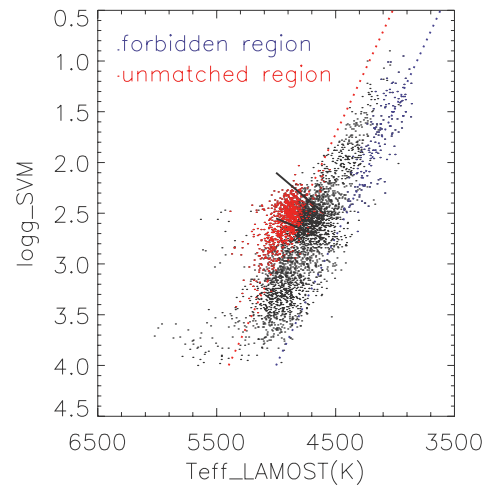
Fig. 7 A comparison of the T_{eff} versus $\log g$ diagram based on new gravities from Liu et al. (2015, submitted to ApJ). The symbols are the same as in the upper left panel of Fig. 4.

It is interesting to investigate how stars in the forbidden and unmatched regions in Figure 5 behave with these new gravities. Figure 7 shows the T_{eff} versus $\log g_{\mathrm{SVM}}$ diagram for 4915 stars. Interestingly, most stars in the forbidden region (blue dots) are located around the blue dashed line, on the right side of which the APOGEE dataset is lacking stars. Clearly, new gravities from Liu et al. (2015, submitted to ApJ) seem to be more reasonable and they are consistent with those in the APOGEE dataset in this region within the errors. Moreover, a substantial number of stars in the unmatched region in Figure 5 are located in the left part of the main RC stars, indicating that they are probably also main RC stars instead of secondary ones. In addition, the main feature of RC stars becomes quite prominent in the T_{eff} versus $\log g_{\mathrm{SVM}}$ diagram as stars in the unmatched region of Figure 5 are included. However, the selection of RC stars within the two black lines may not be

Fig. 8 A comparison of the slopes in the $T_{\rm eff}$ versus $\log g$ diagram for RC stars with new gravities from Liu et al. (2015, submitted to ApJ), the LAMOST dataset and the SAGA survey by Casagrande et al. (2014).

suitable based on new gravities. Instead, there is not a significant dependence of $\log g$ on $T_{\rm eff}$ for the main RC feature.

In Figure 8, we plot the $T_{\rm eff}$ versus $\log g_{\rm SVM}$ diagram for our selected RC sample of stars with [Fe/H] > -0.5. The slope is 0.18 dex per 1000 K which is consistent with that from the SAGA survey by Casagrande et al. (2014).

4 SUMMARY

We have compared differences between the LAMOST and the APOGEE datasets in the stellar parameters $T_{\rm eff}$, $\log g$ and [Fe/H]. We have identified the main sequence of RC stars in the $T_{\rm eff}$ versus $\log g$ diagram from the LAMOST dataset, which behaves in a more reasonable way than that from the APOGEE dataset. For RGB stars, the LAMOST dataset spans a wider range than the APOGEE dataset in the $T_{\rm eff}$ versus $\log g$ diagram, and a group of stars with $2.6 > \log g > 0.00253 \times T_{\rm eff} - 8.67$ is located in a forbidden region where no theoretical model predicts stellar parameters can exist. We further exclude stars that have a metallicity of [Fe/H] > -1, which does not match their positions in the $T_{\rm eff}$ versus $\log g$ diagram (outside the blue dashed line where RGB stars with [Fe/H] < -1 are located).

We have established a good metallicity calibration of $[{\rm Fe/H}]_{\rm APOGEE} = 1.18 \times [{\rm Fe/H}]_{\rm LAMOST} + 0.11$ ($\sigma = 0.08$) for both RC and RGB stars, and a temperature calibration of $T_{\rm eff,APOGEE} = 0.95 \times T_{\rm eff,LAMOST} + 210$ ($\sigma = 53$ K) in consistent with the one-to-one line within the measured errors. There is no clear trend in gravity between the LAMOST and the APOGEE datasets for RC stars, and we may prefer the LAMOST dataset rather than the APOGEE dataset since the former follows the general trend of increasing $\log g$ with decreasing $T_{\rm eff}$, which is a feature of RCs that is seen in the CMD of local RC stars in the field and some old open clusters. For example, the CMD of an old open cluster NGC 6819 in Lee-Brown et al. (2015) shows that the V magnitude becomes fainter (corresponding to a decrease in luminosity) as the $(B - V)$ color becomes redder (indicating a decrease in temperature). However, the RC sample of Casagrande et al. (2014) does not show this dependence, and we need further study to clarify if the dependence of $\log g$ on $T_{\rm eff}$ for RC stars is true. For RGB stars, we prefer calibrations of $\log g_{\rm APOGEE} = 0.000874 \times T_{\rm eff,LAMOST} + 0.588 \times \log g_{\rm LAMOST} - 3.117$ ($\sigma = 0.167$) for [Fe/H] < -1 and $\log g_{\rm APOGEE} = 0.000615 \times T_{\rm eff,LAMOST} + 0.697 \times \log g_{\rm LAMOST} - 2.208$ ($\sigma = 0.150$) for [Fe/H] > -1 after excluding stars in the forbidden region and the unmatched region of the $T_{\rm eff}$ versus $\log g$ diagram. Finally, we have found that new gravities from the SVM method based on the asteroseismic $\log g$ by Liu et al. (2015, submitted to

ApJ) are more reliable than the original values in the LAMOST dataset for stars in both the forbidden and unmatched regions.

References

Ahn, C. P., Alexandroff, R., Allende Prieto, C., et al. 2012, ApJS, 203, 21

Bovy, J., Nidever, D. L., Rix, H.-W., et al. 2014, ApJ, 790, 127

Bressan, A., Marigo, P., Girardi, L., et al. 2012, MNRAS, 427, 127

Casagrande, L., Silva Aguirre, V., Stello, D., et al. 2014, ApJ, 787, 110

Cui, X.-Q., Zhao, Y.-H., Chu, Y.-Q., et al. 2012, RAA (Research in Astronomy and Astrophysics), 12, 1197

De Cat, P., Fu, J. N., et al. 2014, astro-ph/1411.0913

Eisenstein, D. J., Weinberg, D. H., Agol, E., et al. 2011, AJ, 142, 72

Girardi, L. 1999, MNRAS, 308, 818

Holtzman, J. A., Shetrone, M., Johnson, J. A., et al. 2015, arXiv:1501.04110

Huber, D., Silva Aguirre, V., Matthews, J. M., et al. 2014, ApJS, 211, 2

Kordopatis, G., Gilmore, G., Steinmetz, M., et al. 2013, AJ, 146, 134

Lee-Brown, D. B., Anthony-Twarog, B. J., Deliyannis, C. P., Rich, E., & Twarog, B. A. 2015, AJ, 149, 121

Liu, X. W., Zhao, G., & Hou, J. L. 2015, RAA (Research in Astronomy and Astrophysics), 15, 1089

Pinsonneault, M. H., Elsworth, Y., Epstein, C., et al. 2014, ApJS, 215, 19

Puzeras, E., Tautvaišienė, G., Cohen, J. G., et al. 2010, MNRAS, 408, 1225

Stello, D., Huber, D., Bedding, T. R., et al. 2013, ApJ, 765, L41

Wu, Y., Luo, A., Du, B., Zhao, Y., & Yuan, H. 2014, arXiv:1407.1980 (IAU Symposium No. 306, in press)

Yanny, B., Rockosi, C., Newberg, H. J., et al. 2009, AJ, 137, 4377

Zhao, G., Zhao, Y.-H., Chu, Y.-Q., Jing, Y.-P., & Deng, L.-C. 2012, RAA (Research in Astronomy and Astrophysics), 12, 723